Journal Name

ARTICLE TYPE

Cite this: DOI: 00.0000/xxxxxxxxxx

Computational Methods of Visualising Aromaticity and Antiaromaticity in Macrocycles

Dylan Morgan[a]

Received Date
Accepted Date

DOI: 00.0000/xxxxxxxxxx

Visualisation of molecules for publication is of underestimated importance, but can often provide a meaningful and descriptive insight of work conducted; if executed well. This is especially true for large and complex macrocycles that are aromatic, antiaromatic, or some combination of the two. Whilst there is currently promising research being conducted to formalise a method to enable better visualisations, said research is limited and there is scope for improvement in current methods. In this literature review, some background in computational chemistry is firstly provided to understand the basic process by how molecules can be represented in a visual form, followed by older, commonly used, and widely accepted methods of mapping aromaticity quantitatively, as well as newer, more advanced techniques. Some examples of how these techniques are currently being applied in literature to realise the complicated aromatic/antiaromatic behaviour of certain new compounds are also covered.

Contents

[a] *Department of Chemistry, Loughborough University, Loughborough, Leicestershire, LE11 3TU. E-mail: d.morgan-16@student.lboro.ac.uk*

1 Introduction

Arguably, the first useful computational chemistry methods for solving the Schrödinger equation for many-bodied systems were developed in the 1990s, and since then, the use of computers to perform chemical calculations has increased significantly in the last 30 or so years.[1–3] It has become a widely used tool in many fields within chemistry, from predicting reaction pathways through transition state geometry and vibrational analysis, to development of methods on quantum computers to model highly correlated systems.[4,5]

The creation of graphics and inclusion of visual descriptors is an often overlooked and underestimated means for the communication of information - even when used in a qualitative manner. As aromaticity is an inherently difficult phenomenon to quantify, as the almost innumerous number of publications and definitions available on the topic spanning over 150 years will testify to, even qualitative visualisations provide an easily accessible means for most people to quickly attain structural information about.[6] Additionally, understanding of the calculations which are ordinarily performed in quantum chemistry on aromatic compounds is something that anyone short of a degree in chemistry, computer science, and mathematics will probably find challenging to understand (as I can personally attest to)!

Before delving into the different methods and techniques of visualising aromatic molecules, some domain knowledge firstly needs to be understood. A very brief background will be given on aromaticity hereafter in section 2.1, then some essential computational chemistry will be discussed for the remainder of the background in section 2.2. Then, in section 3 we will look at the main visualisation methods that have been developed over

the last 25 years, including nucleus-independent chemical shift, anisotropy of the induced current density, and commonly used variants of these methods. As will be shown in section 4, there have been a number of papers published in recent years where at least a significant portion of the research has revolved around interesting macrocycles that either contain local regions of aromaticity and/or antiaromaticity, are able to switch between being locally and globally aromatic or antiaromatic, or are aromatic or antiaromatic in 3D and are not simply fully planar molecules.

2 Background

2.1 Aromaticity vs. Antiaromaticity

Aromaticity is a phenomenon observed in a range of compounds and is a highly important concept in organic chemistry, being a characteristic feature of many molecules. It is also a concept where a true understanding was elusive for many years, and thus has been a subject of immense and exhaustive study, ranging from Kekulé's first proposition to explain some of the unusual characteristics of benzene, to the preposition and eventual acceptance of ring currents. [7,8]

There are many issues that present themselves when attempting to quantify the degree by which a molecule is aromatic. This has led to many descriptors of what aromaticity actually is and attempts at quantifying it. [7,9] That being said, Hückel's rules are widely used as a definition of aromatic molecules, and are outlined as follows: [10]

1. Molecule is cyclic
2. Each atom in the ring retains 1 $2p_z$-orbital whilst the others form part of an sp^2 hybridized planar ring
3. $4n+2$ electrons in π orbitals where $n \in \mathbb{N}_0$

As a note on point 3, this formula refers to a sequence. In other words, if the number of π electrons in a molecule corresponds to $4n+2$, where n is any positive integer, the molecule is aromatic. For example, benzene contains 6 π electrons, and when $n=1$, $4n+2=6$, therefore is aromatic. Cyclobutadiene by comparison contains 4 π electrons, and there is no value of n that is a positive integer which satisfies $4n+2=4$.

Antiaromaticity refers to another category by which a molecule can be classified by. They largely adhere to the same criteria as aromatic compounds, aside from point 3 - where instead of $4n+2$, they have $4n$ π electrons. [11] These molecules, for instance cyclobutadiene, are extremely unstable and near-impossible to isolate, owing to their tendency to dimerise and undergo Jahn-Teller distortions as frontier molecular orbitals attempt to align. [12–15] In a physical sense, antiaromatic compounds can be thought of as aromatic compounds on the verge of losing their aromaticity. Whilst many antiaromatic molecules simply do not exist at all or at least not at room temperatures, as will be shown in section 4, there are examples where they are stable and have practical applications.

2.2 General Computational Chemistry

Quantum mechanics plays an important role in computational chemistry, and provides the basis of all *ab inito* calculations that are conducted. In order to understand how molecular structures can be computed and visualised, we must first venture into the theory behind how these calculations are performed. This is not to provide a background on all quantum chemistry, and some basic knowledge on maths and quantum chemistry is assumed, but rather the following sections 2.2.1 to 2.2.3 explain how these concepts are applied in the context of computational chemistry.

2.2.1 Hartree-Fock and Self-Consistent Field Theory

There are several levels by which theoretical chemistry calculations can be performed, ranging from the most accurate but also expensive *ab initio* techniques to force-field gradients which are ordinarily reserved for large proteins and bio-molecules. Hartree-Fock and self-consistent field (HF-SCF) were the first *ab initio* techniques to calculate the shape of electronic orbitals. [16,17]

The electronic wavefunction Ψ is a product of the spatial coordinates of all electrons X_n in a system and their spin multiplicities ϕ_n, where n is the number of electrons in the system. If the wavefunction is written out simply like (2.1) as a Hartree product, anti-symmetry of the wavefunction is not satisfied, and doesn't comply with the Pauli principle. [18]

$$\Psi(X_1, X_2, ..., X_n) = \phi_1(X_1)\phi_2(X_2)...\phi_n(X_n) \tag{2.1}$$

By writing the wavefunction as a Slater determinant, as in (2.2), anti-symmetry can be maintained in a wavefunction with n components:

$$\Psi(X_1, X_2, ..., X_n) = \frac{1}{\sqrt{n!}} \begin{vmatrix} \phi_1(X_1) & \phi_2(X_1) & \dots & \phi_n(X_1) \\ \phi_1(X_2) & \phi_2(X_2) & \dots & \phi_n(X_2) \\ \vdots & \vdots & \ddots & \vdots \\ \phi_1(X_n) & \phi_2(X_n) & \dots & \phi_n(X_n) \end{vmatrix} \tag{2.2}$$

The energy of a Slater determinant is made up of the following terms: electronic kinetic energy, electron-nucleus attraction, nucleus-nucleus repulsion, and electron-electron repulsion. The latter is further split into a coulombic interaction (electrostatic repulsion due to like charges) and the non-local exchange interaction (anti-symmetry nature of the wavefunction), however division of inter-electronic repulsion into these terms gives rise to an error, dubbed electron correlation. [19] This will be addressed later in section 2.2.2. Through construction of the Slater determinant, the wavefunction is able to be solved.

Self-consistent field theory (SCF) is a direct extension of Hartree-Fock, and is an iterative method used in quantum chemistry calculations which finds the shape of the orbitals that minimise the energy of the Slater determinant. [20] This problem has to be solved iteratively as the electron density is a function of the shape of the orbitals, and can be well optimised for use on a computer. Firstly, an initial guess of the electron orbitals and energies is made by the algorithm of the program. From this, the electron density can be obtained, then the Hartree-Fock equations can be solved to correct the initial guess of the orbitals and energies. The orbitals and energies are re-calculated and updated based off the new values and the process repeats, resulting in convergence until the change in energies reaches a value specified in the algorithm,

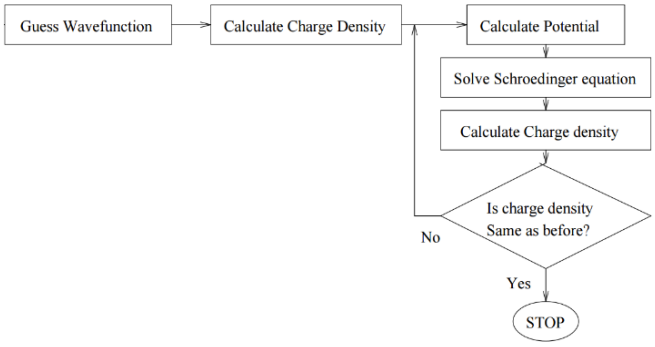

Fig. 1 Algorithm that SCF uses to minimise the energy of the Slater determinant and obtain the shape of the molecular orbitals.[21]

whereby the process will complete.[21]

2.2.2 Density Functional Theory

Post-Hartree-Fock methods were developed as a result of inaccuracies accrued through lack of consideration of electron correlation. Despite the percentage error being relatively small, the error can be magnified in certain situations.[22] They are excellent for determining highly accurate models of chemical systems, however calculations of such a nature were (and often still are) too expensive for all but the smallest molecules - especially on hardware of that period.

Density functional theory (DFT) was optimised for use in computational chemistry in the 1990s and provides a more feasible alternative for many chemists to post-Hartree-Fock methods for calculating structures in the majority of instances without requiring access to state-of-the-art hardware. Lee et al.[1] and Becke[2] released in 1988 and 1993 their papers on electron correlation and exchange energy to develop the revered B3LYP functional, arguably projecting DFT into the level of popularity it now sees. Today, DFT makes up of nearly 80% of all computational chemistry calculations and as a result, the papers by Lee et al. and Becke are some of the most cited papers of all time, as of 2014.[23,24]

By mapping the total energy of a system as a functional (ie. a function of another function) of the electron density, the internuclear and electron-nuclear repulsion can be easily mapped to obtain the Hamiltonian. This approach solves the Schrödinger equation without having to calculate the wavefunction.[25] However the electronic kinetic energy $\hat{T}_e$ and electron-electron repulsion V_{ee} cannot be accurately obtained in this way. The electron-electron repulsion can be further split into the coulombic repulsion between electrons E_{coul}, exchange energy (anti-symmetry of the wavefunction), and correlation energy (interaction of many electrons). An approximation called the exchange-correlation E_{xc} functional is used as a workaround for this. There are many different designs of such a functional, but principally fall into one of the following three categories:

- Local density approximation (LDA)
- Generalised gradient approximation (GGA)
- Hartree-Fock exchange, often known as hybrid functionals

LDA functionals were developed first but are prone to significant error as they map the electron density uniformly across a molecule, whereas GGAs correct this by also considering the gradient of the density.[26] For the purposes of visualising macrocycles, PBE0 is a hybrid functional often used in geometry optimisation and NICS calculations (see section 2.2.3 and 3.1), meaning simply that contributions for the correlation energy are primarily obtained from DFT for faster calculations, but at least some contributions also come from HF methods, so appropriately high accuracy is maintained.[27] PBE0 specifically takes 25% of its exchange energies from HF $E_X(HF)$ and 75% from the GGA based PBE functional $E_X(PBE)$, plus the correlation term which is dealt with by another GGA functional - mPW91 $E_C(mPW91)$.[26,28] As such, the calculation of the exchange correlation term in PBE0 is given by (2.3).[29]

$$E_{XC} = 0.25E_X(HF) + 0.75E_X(PBE) + E_C(mPW91) \tag{2.3}$$

An approach using Kohn-Sham DFT enables the kinetic energy to be solved by using orbitals to construct the density. The 'standard' DFT approach to the electronic energy is given by (2.4), and the Kohn-Sham DFT is shown in (2.5). E_e is the electronic energy, E_{kin} is electron kinetic energy obtained from conventional quantum theory, E_{ext} is the external potential energy, and $E_{kin,KS}$ is the energy of non-interacting Kohn-Sham orbitals.

$$E_e = E_{kin} + E_{coul} + E_{xc} + E_{ext} \tag{2.4}$$

$$E_e = E_{kin,KS} + (E_{kin} - E_{kin,KS}) + E_{coul} + E_{xc} + E_{ext} \tag{2.5}$$

2.2.3 Geometry Optimisations

When creating visuals of molecules using computational methods, the geometry of the molecule of interest first needs to be optimised. This is an often trivial task and one of the most fundamental in computational chemistry, and must be completed before obtaining any further desired information about the molecule. The method to achieve this is outlined as follows; an initial structure is drawn in a molecular editor, where it is pre-optimised using force-field methods often built in to the editor. Some examples of commonly used molecular editors are Avogadro and Jmol.[30,31] In the case of Avogadro, gaff and MMFF94 force-field methods are available and recommended for organic molecules, of which are employed from OpenBabel.[32–35] Once the pre-optimisation has completed, the atomic coordinates can then be exported and written into the input file of a quantum chemistry program. Before running the job, the functional, basis set, and type of job need to be specified and written in the appropriate syntax for the program. Finally, the job can be run which will generate an output of the molecule. Jmol or Avogadro can be used for visualisation of the output, but there are also more specialised programs available, such as Molden.[36] The force fields methods employed by molecular editor programs are scarcely adequate enough for geometry optimisations as they only calculate geometries through intramolecular steric interactions and do not take in to account quantum effects, and is often especially apparent in aromatic compounds.

Mathematically, a geometry optimisation will follow a theoret-

ical potential energy surface (PES), like in **figure 2** and (2.8).[37] The energy is a function of all coordinates of the PES. This is made up of peaks and troughs which correspond to local energy maxima and minima conformations of the molecule. When optimising a geometry, the Born-Oppenheimer approximation can be applied, where the contribution of the nuclear kinetic energy to the Hamiltonian $\hat{H}$ is disregarded. This simplifies the calculation greatly with a very minor decrease in accuracy, and gives rise to the electronic Hamiltonian operator $\hat{H}_e$ (2.6) which is the sum of the electronic kinetic energy-operator $\hat{T}_e$, electron-electron repulsion V_{ee}, electron-nucleus attraction V_{ne}, and nucleus-nucleus repulsion V_{nn}.[38]

$$\hat{H}_e = \hat{T}_e + V_{ee} + V_{ne} + V_{nn} \tag{2.6}$$

To obtain nuclear geometries R, the electronic Schrödinger equation must be solved for R, where $\Psi(r;R)$ is the electronic wavefunction at R, and $E(R)$ is the energy at R (2.7).

$$\hat{H}_e\Psi(r;R) = E(R)\Psi(r;R) \tag{2.7}$$

$$E = E(R) = E(X_1, Y_1, Z_1, ..., Z_N) \tag{2.8}$$

Through 1st and 2nd partial differentiation of $E(R)$ of all coordinates across a PES, the nature of the coordinates can be ascertained. The 1st derivative is referred to as the gradient vector G and is expressed as a 1D vector of all partial derivatives of the nuclear positions (2.9). The physical interpretation of this can be considered as a force acting on the nuclei.

$$G = \Delta E = \begin{pmatrix} \frac{\partial E}{\partial X_1} \\ \frac{\partial E}{\partial Y_1} \\ \frac{\partial E}{\partial Z_1} \\ \vdots \\ \frac{\partial E}{\partial Z_N} \end{pmatrix} \tag{2.9}$$

$$H = \Delta E = \begin{pmatrix} \frac{\partial^2 E}{\partial X_1 \partial X_1} & \frac{\partial^2 E}{\partial X_1 \partial Y_1} & \cdots & \frac{\partial^2 E}{\partial X_1 \partial Z_N} \\ \frac{\partial^2 E}{\partial Y_1 \partial X_1} & \frac{\partial^2 E}{\partial Y_1 \partial Y_1} & \cdots & \frac{\partial^2 E}{\partial Y_1 \partial Z_N} \\ \frac{\partial^2 E}{\partial Z_1 \partial X_1} & \frac{\partial^2 E}{\partial Z_1 \partial Y_1} & \cdots & \frac{\partial^2 E}{\partial Z_1 \partial Z_N} \\ \vdots & \vdots & \ddots & \vdots \\ \frac{\partial^2 E}{\partial N_1 \partial X_1} & \frac{\partial^2 E}{\partial N_1 \partial Y_1} & \cdots & \frac{\partial^2 E}{\partial N_1 \partial Z_N} \end{pmatrix} \tag{2.10}$$

When taking the 2nd derivative, a 2D matrix is generated as all permutations of the 1st derivative must be accounted for, which is called the Hessian H (2.10). This provides further information about the stationary points - specifically whether it is a local minima or saddle point. If it is a minimum, all partial derivatives will equate to 0, and all eigenvalues square roots of the Hessian will be real numbers. Physically, a minimum represents a product, reagent, or intermediate in a reaction. A saddle point will yield exactly 1 negative square root eigenvalue of the Hessian, which is often described as being an imaginary frequency, and physically represents a transition state. This is because when calculating vibrational modes of the molecule, the square root of the Hessian is taken, and being a negative number, then becomes imaginary.

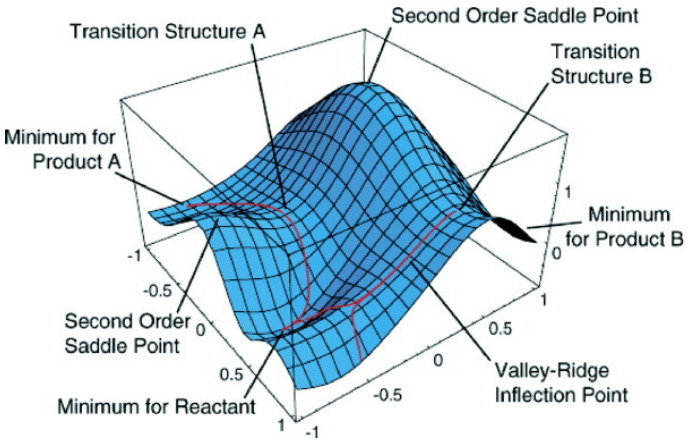

Fig. 2 Example of a potential energy surface showing local energy minima, maxima, saddle points, and reaction pathways (*red*).[37]

In order to obtain the structure of the compound at a local energy minimum, the program will optimise the geometry via an iterative procedure. Using a gradient descent algorithm, a local minima or saddle point will be obtained from the PES.

3 Current Computational Techniques for Visualising Aromatic Compounds

There are a range of techniques currently available which enable computational visualisation of properties of molecules - some specific to aromatic/antiaromatic ring systems, and some more generalised. Nucleus independent chemical shift (NICS) is perhaps one of the most widely used, but others such as anisotropy of the induced current density (ACID), have also found significant traction.[39–41] Whilst these methods may have been around for 20-30 years, they are still widely used today, as we shall see in section 4, and although there haven't been many significant developments since the mid-2000s, there appears to be somewhat of a resurgence of interest of late.

Provided in this section is not a comprehensive review on each method, for that the reader should access the numerous reviews and original research cited here, but rather a summation of each method and some commonly used variations of them.

3.1 Nucleus-Independent Chemical Shift

Nucleus independent chemical shift (NICS) is based on the concept that aromatic and antiaromatic compounds will affect the chemical shift of spin sensitive nuclei. The technique was first published in 1996 by Schleyer et al.,[39] and there have since been several revisions of and appendages to the method, which shall be explored later in this section. However, before exploring the NICS method in more detail, we must first understand the effect of aromaticity on chemical shift in the context of NMR.

A current will induce a magnetic field perpendicular to its direction of flow. If one were to observe - facing head on - to the direction of flow of a current though a wire, the direction of the induced magnetic field would be anti-clockwise. Furthermore, a

magnetic field will also induce a current in a wire. To apply this in a chemical context, the delocalised electrons in cyclic aromatic compounds act in the same way as those in a wire. This is called the ring current model and was first proposed by Linus Pauling, Kathleen Lonsdale, and Fritz London around 85 years ago, which they argued arises as a consequence of $2p_z$ orbital overlap enabling free electron movement around the ring.[42–45] In an NMR instrument, the applied magnetic field instigates a flow of the electrons when perpendicular to the ring. Ordinarily in planar aromatic compounds the ring current flows anti-clockwise (diatropic), which induces another magnetic field that opposes the applied field, causing any atoms situated outside the ring to become more deshielded and to give rise to chemical shift values that are more positive, for example benzene in **figure 3**.[46–49] Conversely, inside the ring, the induced magnetic field enhances the applied field and therefore causes atoms in the proximity of the field to experience additional shielding.[7,50]

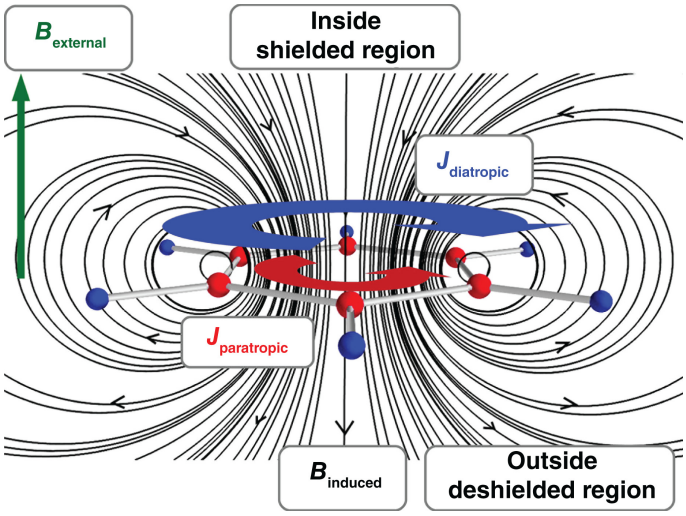

Fig. 3 Illustration of the diatropic ($J_{diatropic}$, blue) and paratropic ($J_{paratropic}$, red) ring currents present in benzene and the induced magnetic fields $B_{induced}$ when a magnetic field is applied perpendicularly $B_{applied}$, originally published by Sundholm et al.[49]

The opposite effect is observed in antiaromatic compounds, whereby the ring current flows in the reverse direction (paratropic). The induced currents are therefore complimentary outside the ring and opposing inside, causing opposite shielding/deshielding effects of substituents to aromatic molecules. It is also one of the easiest ways to computationally determine whether a molecule is aromatic or antiaromatic, as was first proposed by Schleyer et al., and is outlined as follows.[39] The molecule of interest is firstly optimised in such a manner as was discussed in section 2.2.3. In addition to obtaining an accurate structure of the molecule, this is also an important step as the program used will centre the atomic coordinates around the origin. The updated grid coordinates can then be parsed from the output file to a new input file, and virtual atoms, or ghost atoms as they are often referred to as and denoted as 'Bq', are appended to the end of the input file. Ghost atoms don't have any influence on the electronics or sterics of the rest of the structure, and purely serve as a reference point of which the isotropic chemical shifts values can be measured from. By running an NMR calculation on the new input file, these values can be obtained.

Where the Bq atoms should be placed when performing the calculations was a matter of debate throughout the early 2000s. Originally, NICS was measured from in-plane contributions at the ring centre, NICS(0), although this was later shown to be prone to error, thanks to contributions from the σ molecular orbitals.[51,52] By simply recording the NICS values 1 Å above the ring plane, where the density of the delocalised π electrons are at their highest density, the effect of the σ orbitals is made negligible.[53]

There have been many assessments over the years as to which NICS technique provides the greatest accuracy.[54–56] The most effective manner in which NICS should be used is to not rely on any single technique, but rather to utilise several and assess the results critically based on the molecule in question.[57] Considering the ease by which computations of this nature can be performed in 2021, this should be a relatively computationally inexpensive task for most molecules.

Perhaps surprisingly, given the widespread-usage of the NICS method, there has been little in the way of advancements and developments in using the technique, for instance, the use of generating a grid of ghost atoms has been in use since at least 2001.[53,58] That being said, there has been somewhat of a renewed interest in recent times, with section 4.2 discussing how a NICS based visualisation method was used to determine the nature of aromaticity in norcorroles, and there is certainly an aperture in the literature for a more updated and modern technique.

3.1.1 NICS Probe in the Z-Plane

A paper published in 2006 by Amnon Stanger[59] recognised some of the shortcomings of the then-standard NICS(0) and NICS(1) processes. At the time, it was considered that the lower the isotropic magnetic shielding, the more aromatic the molecule. However, in certain instances such as with anthracene, it was claimed that "that the central ring in anthracene was more aromatic than the terminal ring".[53,59] This infers that there would be a difference in reactivity between central and terminal rings, however this isn't corroborated with experimental observations, as "Anthracene undergoes an electrophilic attack at the 9 position, and the 9 and 10 positions also undergo Diels-Alder reactions, which are indicative of conjugated nonaromatic systems", as stated by Stanger.[59] He also gives more examples of such instances in his paper on some of the incorrect conclusions that can be drawn from NICS(1) derived computations.

What Stanger proposed in his paper is that by taking a range of NICS values bisecting the z-axis increasing in value from the centre of the molecular plane, the level of aromaticity could be separated into the in- and out-of-plane contributions. This may be from the origin to approximately 5 Å out. Presented by him is this method applied to a range of compounds of which have greater congruency with other computational and experimental techniques. Examples of the differences in NICS-z to NICS-in-plane is shown in **figure 4** with benzene and cyclobutadiene.

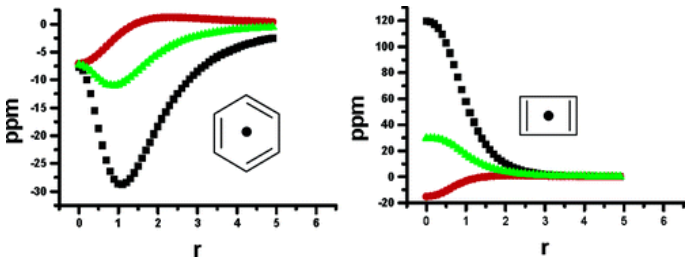

Fig. 4 Difference in NICS values for benzene and cyclobutadiene obtained through in-plane (*red*) and out-of-plane (*black*) methods as a function of distance (r), where out-of-plane NICS bisects the centre of each molecule. This is compared to the isotropic chemical shift (*green*). Out-of-plane NICS shows a much greater chemical shift (ppm) for both diatropic benzene and paratropic cyclobutadiene.[59]

3.1.2 Isotropic Magnetic Shielding of PAHs

As aromaticity is inherently difficult to quantify and has many different descriptors, not all computational methods are based off of Hückel's definition. Clar's sextet model is often used when considering poly-aromatic hydrocarbons (PAHs), where a sextet refers to 6 delocalised π electrons, normally represented by a circle in a molecule such as benzene. More specifically, the dominant resonance form of a PAH is represented by the form containing the greatest number of sextets, for example in **figure 5**.[60–63] Erich Clar essentially pioneered the field of PAHs throughout his much of his career in the 1950s - 1970s, and was responsible for the synthesis and characterisation of many of them.[64]

The requirement of a method to assess aromaticity is being realised, as Lamkin et al. very recently published a NICS(1)-based method to do so.[63] By obtaining NICS(1) isotropic magnetic shielding values $\sigma_{iso}(r)$ across the xy plane of the PAH phenanthrene, they were able to map $\sigma_{iso}(r)$ to an contour plot, where darker regions represent higher chemical shift. By overlaying the contour plot with the skeletal molecular structure across various PAHs, they were able to verify the accuracy of Clar's sextet model, in that the dominant resonance forms were correctly predicted by sextet theory, as in **figure 5**. Furthermore, **figure 5** also demonstrates there is presence of the non-dominant resonance form, as the highly aromatic regions do not connect fully on the outer rings, and are also evident on the middle ring.

3.2 Anisotropy of the Induced Current Density

Anisotropy of the Current (Induced) Density (ACID) differs from NICS by computing paramagnetic anisotropic delocalised electron current density as opposed to predicting values for chemical shift. This enables a wider scope for its use, as it's not restricted to just visualisation of cyclic compounds, but also conjugated alkenes and enolates, to name a few examples.[65] If ACID used current density directly, measurements would have to be obtained from 1 Å above the plane, like NICS. This is because current density arises from both local currents contributed by individual atoms, and interatomically otherwise.[66] To further complicate matters, the local currents "where the electrons occupy atom-centered orbitals are several orders of magnitude larger than the so-called interatomic currents" and "currents in π systems vanish in the nodal plane".[41] Instead, by removal of all diamagnetic contributions, which are "a function of the total linear electron density", the purely paramagnetic contributions remain, and thus only the interatomic currents remain represented, as was determined and calculated by Rainer Herges and Daniel Geuenich in 2001.[40,41]

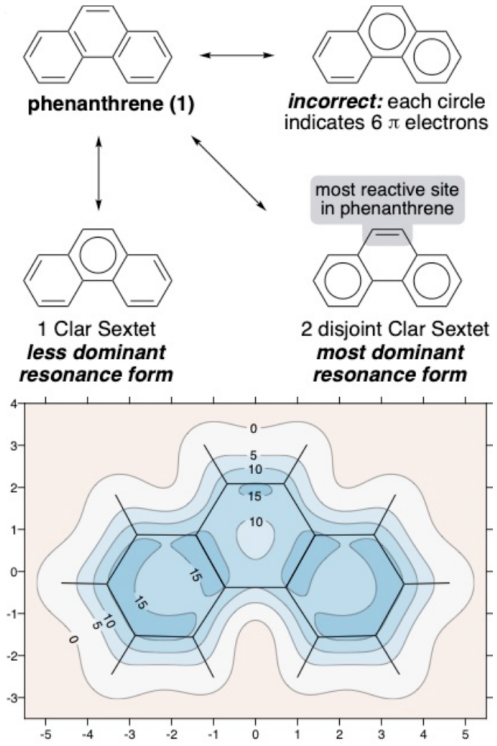

Fig. 5 Example given by Lamkin et al. of their NICS(1)-based isotropic magnetic shielding method of visualising PAHs using phenanthrene (*bottom*), and how it closely resembles the theorised Clar Sextet model of PAHs. Also displayed (*top*) are the correct and incorrect resonance forms of phenanthrene using Clar sextets, and prediction of its most dominant resonance form.[63] The numbers on the graph represent $\sigma_{iso}(r)$ values and axis are distances in Å.

Once the values for the individual points have been calculated, they can be plotted as a scalar field isosurface, where the distance between points can be specified arbitrarily. An isosurface is simply a 3D plot where every value is a constant, analogous to a contour graph in 2D.[67] Scalars are numbers that aren't vectors, can represent a vector in vector space, and have magnitude but not direction. For instance, a vector $\vec{v}$, can be represented by the scalars x and y, as (x,y). In Gaussian, when computing ACID isosurface values, the total current density is calculated using continuous set of gauge transformation CSGT method developed by Bader et al.[41,68–71]

4 Applications of Techniques

Today, one of the most useful applications of most of the techniques outlined in section 3 is in generating diagrams for and visualising aromatic/antiaromatic regions of complex macrocycles. ACID and GIMIC are most often used to achieve this, however when applied as standard, may not always provide the clearest

visualisations, leaving scope for the development of a new and better method, as will be shown further in greater detail in sections 4.1 through 4.3.

Unfortunately, only a small selection of applications for such techniques are able to be mentioned here, but have been selected from a wide breadth of applications and fields, as well as interesting and not-seen-before examples of aromatic compounds.

4.1 New Electrodes for Sodium Ion Batteries

Lithium ion batteries (LIBs) and their many variants are a technology that have revolutionised modern electronics and electric cars. They were first commercially introduced in 1991 and have become exceedingly popular primarily thanks to the relatively high charge storage capacity per unit mass or volume (energy density) they can deliver, and their abstinence for consumption of the electrolyte.[72] As a consequence, they are able to undergo many charge-discharge cycles.[73,74] However, LIBs don't come without their drawbacks; lithium is an unsustainable and finite resource, combustible in air, and expensive.[72,75]

Sodium-ion batteries (SIBs) present an exciting alternative for some applications that LIBs are currently used for. They don't suffer from many of the same drawbacks as LIBs, as sodium is a significantly more abundant and cheaper resource, however compromise on their charge density and performance. Due to this, one of the most anticipated application of SIBs includes large-scale energy storage[76–78]. Historically, SIBs were co-developed alongside LIBs, however development was all but halted when a material that was suitable for electrodes and was stable over many charge-discharge cycles could not be found.[79] In recent years, there has been somewhat of a resurgence of interest in SIBs as a more cost effective alternative to LIBs is desired, and there has been progress into finding an appropriate material for SIB electrods.[80] One such prospect can be found in an article published in 2020 by Eder et al.[81] They uncovered a next-generation material called [2.2.2.2]paracyclophane-1,9,17,25-tetraene (PCT) which can "stabilize the neutral state by local aromaticity and the doubly reduced state by global aromaticity, resulting in an anode material with extraordinarily stable cycling performance and outstanding performance under fast-charge/discharge conditions, demonstrating an exciting new path for the development of electrode materials for SIBs and other types of batteries".[81]

In the paper released by Eder et al.[81] they include a structural drawing of an ACID plot of PCT and PCT^{2-}, and show how reduction and oxidation of the macrocycle causes it to switch between having 4 distinct locally aromatic aryl groups and global aromaticity around the entire structure (see **figure 6**). The ACID plot shows areas of electron density around PCT and PCT^{2-} but lacks clear definition between the different states, with manually added arrows around the different aromatic regions to show the direction of ring currents, which are not computationally generated and therefore not a quantitative measurement. A NICS based visualisation method could be employed here, which would only show the regions of aromaticity and not electron density across the entire macrocycle. Furthermore, this would also make apparent the degrees by which the different regions of PCT are aromatic and would leave scope for comparison to the degree of which PCT^{2-} is aromatic.

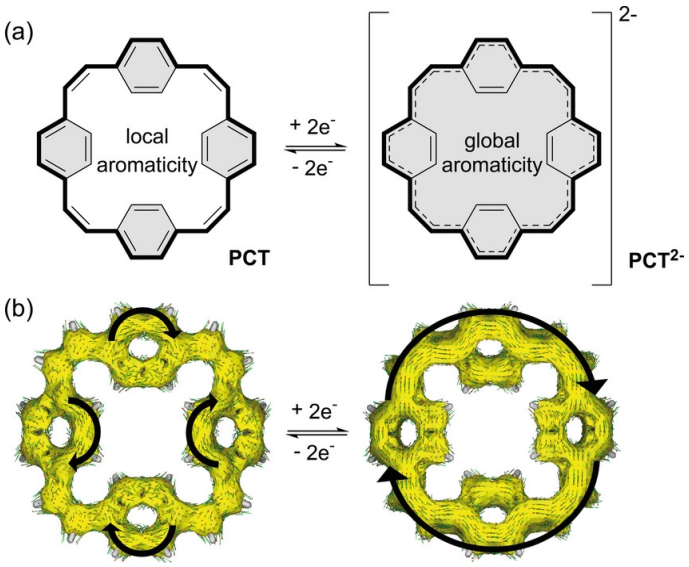

Fig. 6 Example of the ACID plot (b) used by Eder et al.[81] to show how PCT switches to PCT^{2-} and back; transitioning from containing areas of local aromaticity (*left)* to being in its globally aromatic state through oxidation (or reduction for the reverse reaction) (*right*), and a structural drawing to more clearly show these regions (a).

4.2 Determining the Aromaticity of Norcorroles

Porphyrins are a class of compounds that have been around for some time.[83,84] They are incredibly important biologically, with haems and chlorophylls being some of the most well known examples.[85,86] However, the simplest analogues of these was known about only theoretically, until the accidental synthesis of iron norcorrole in 2008 by Martin Bröring et al.[87] as a side product of an oxidative macrocyclisation reaction. nickel norcorrole was then synthesised, isolated, and characterised in 2012 with impressive yields by Ito et al.[88] Interestingly, they also announced it as being particularly "stable under air at room temperature" and "similar to other porphyrin complexes [in regard to their ease of which they are able to be isolated]". This was surprising as Hückel's rule predicts norcorroles to be of antiaromatic nature, which is verified by Ito et al.[88] experimentally. In contradiction to this, DFT calculations had predicted norcorrole to be a nonaromatic polyenic molecule.[89] At this point it is clear there is some discrepancy between theoretical DFT calculations and experimental observations, however further DFT studies conducted in 2019 corroborated the results of the experimental 2012 paper, instead attributing their findings which are traditionally inconsistent of antiaromatic systems to the stability of the dipyrrin halves of the molecule (a dipyrrin is a 2-methylpyrrole connected through a double bond to a 2H-pyrrole, and makes up half of the structure of a norcorrole ring).[90,91] **Figure 8** shows a comparison of dipyrrin, norcorrole, and Ni norcorrole. Additionally, Pd coordinated norcorroles have also been synthesised, and reported as antiaromatic.[92]

As recently as October 2020, the decade and a half long conun-

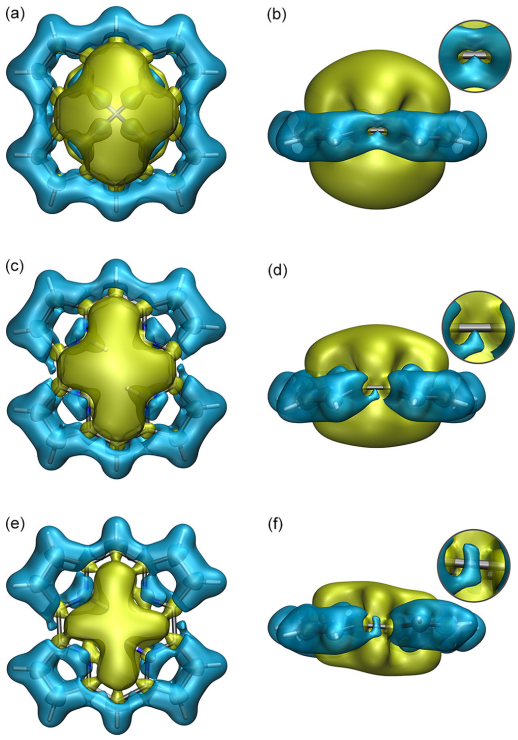

Fig. 7 Antiaromatic regions are denoted by yellow shading, and aromatic by blue. Nickel norcorrole top view (a) and side view (b). (c,d) and (e,f) show the same for norcorrole in different conformations, differentiated by symmetry elements C_2 and C_i respectively.[82]

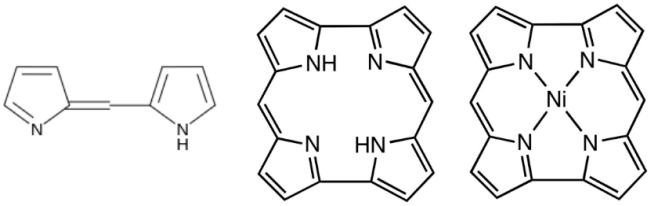

Fig. 8 Comparison of structures of dipyrrin (*left*), norcorrole (*centre*), and Ni norcorrole (*right*).[90]

drum has had new light shed on what exactly transpires in norcorroles. Using DFT and NICS based methods to perform geometry optimisations and differentiate between regions of aromaticity and antiaromaticity, isosurfaces were constructed showing the magnetic shielding tensors around several different PES geometry minima and saddle points of nickel norcorrole and norcorrole, and are shown in **figure 7**.[82,93,94] Karadakov's findings suggest that the norcorroles studied contain an antiaromatic centre surrounded by a "halo" of aromaticity. I wish to place emphasis on the manner in which these conclusions were drawn for the purposes of this review, and are significant in that the nature of these structures have been elucidated exclusively through visualisation-based methods. Complete active space self-consistent field gauge inducing atomic orbitals (CASSCF-GIAO) is a technique used to construct wavefunctions in computational chemistry, and deemed necessary for "the proper description of the magnetic properties of antiaromatic molecules", such as norcorroles.[82] However this method is computationally expensive, and norcorroles are too large and contain too much electron correlation to be feasible on current computer hardware. In lieu of such machines, this visual approach used by Karadakov may be the best and/or only way to verify the true aromatic nature of norcorroles.

The relevancy of such structures may seem questionable, however may be of genuine industrial interest with real applications, and not just a technical exercise. Aromatic-walled 'nanospaces' have already been synthesised, however antiaromatic nanospaces have been sought after but yet remain largely unknown.[95–98]

4.3 3D Aromaticity in Diradicaloid Cages

The final application of aromatic visualisation method discussed in this review is about globally 3D aromatic molecules. Such molecules are scarcely seen in literature, mainly owing to the difficulty of which their synthesis requires, however there are some instances where they can be found, for example cross-conjugated, porphyrin-based, and bridged expanded porphyrinoid cages.[100–105] The molecule c-T12 is a diradicaloid cage that was first synthesised in 2020 by Ni et al, constituting "12 conjugated thiophene units and eight methine linkages".[99] This is the first truly globally aromatic 3D macrocycle to synthesised, and was also able to be oxidised to c-T12^{2+}, c-T12^{4+} and c-T12^{6+}, with cyclic voltammetry confirming the presence of an additional 4 states. Of these, c-T12^{4+} was globally antiaromatic with symmetry C_2, and c-T12^{6+} adopted a D_3 symmetry and was globally aromatic. The final charged and neutral molecules were partially aromatic, but only in 2D. These observations were obtained initially through x-ray crystallographic measurements.

ACID plots shown in **figure 9** substantiated the results obtained experimentally, whereby paratropic ring currents are seen in the globablly antiaromatic c-T12^{4+}, and diatropic currents in the others. Moreover, c-T12^{4+} is unable to undergo significant Jahn-Teller distortions or alter its geometry much to considerably reduce the effect of its antiaromaticity, unlike c-T12^{2+} which should also be antiaromatic but does distort and change to a triplet state to avoid this. DFT confirmed that the weakly aromatic triplet state was indeed lower in energy than the singlet.

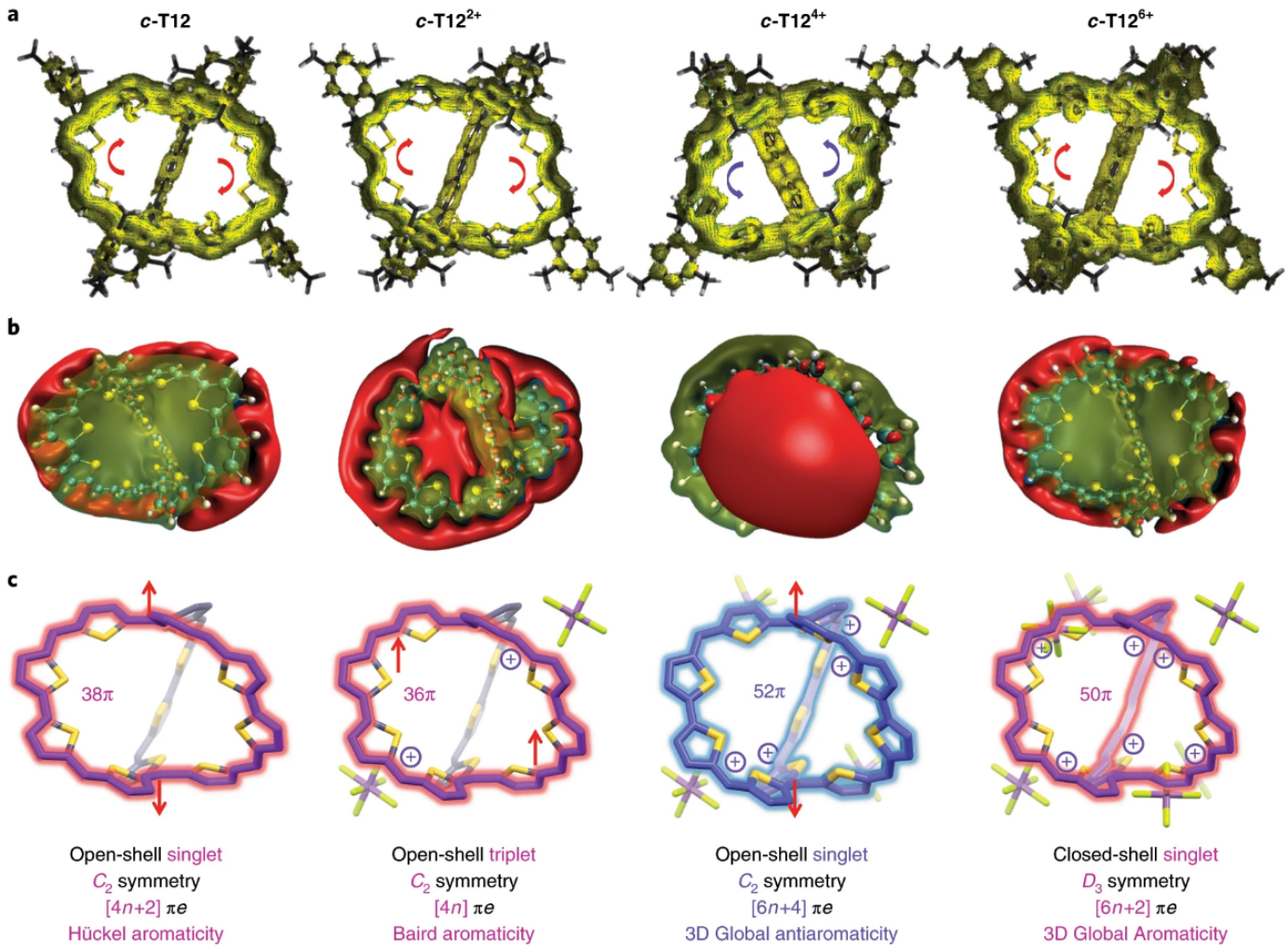

Fig. 9 The different oxidation states of c-T12 shown as an ACID plot (a), a NICS-based visualisation of areas of positive (*red*) and negative chemical shift (*yellow; transparent*): (b), schematic diagrams of aromatic regions of c-T12 to c-T12^{6+} (c), and structural and electronic information about each oxidation state of c-T12.[99]

5 Conclusion and Summarising Remarks

There are a number of methods to visualise macrocycles in the field of computational chemistry, with NICS and ACID being the most commonly found in literature. They have seen widespread use across many fields, ranging from understanding how new electrode materials for sodium-ion batteries are able to switch from containing areas of local aromaticity to being globally aromatic, to the unusual jointly aromatic/antiaromatic character of norcorroles, to the first synthesised globally aromatic 3D compounds. Additionally, there has also been somewhat of a resurgence of research in recent years to further develop these methods and generate better graphics, probably owing to greater advancements in computing power since ACID and NICS were first contrived, and as molecules with more complex aromatic and antiaromatic nature are being synthesised warranting clearer methods of visualisation.

Despite several papers having been released containing such plots of complex aromatic structures, there hasn't yet been a readily accessible, formal method published to visualise 3D aromatic and antiaromatic compounds. Whilst Lamkin et al.[63] have published one such technique, this was only shown with polyaromatic hydrocarbons, and is limited by its restriction of visualising 2D surfaces. A method based around the already widely used and accepted NICS, where isotropic chemical shift values are obtained from a 3D array of ghost atoms and plotted on an isosurface, could be one such candidate for a method to do so. In any event, as observed from the examples given here, there is a need for such a technique to be available in the computational chemistry domain.

6 Acknowledgements

I wish to express thanks to Dr Felix Plasser for academic support and advice.

6 References

1 C. Lee, W. Yang and R. G. Parr, *Phys. Rev. B*, 1988, **37**, 785–789.

2 A. D. Becke, *J. Chem. Phys.*, 1993, **98**, 5648–5652.

3 N. R. Council, D. o. E. Sciences, P. Sciences, M. A. on Physical Sciences and C. Chemistry, *Mathematical Challenges from Theoretical/Computational Chemistry*, National Academies Press, 1995.

4 P. L. Bhoorasingh and R. H. West, *Phys. Chem. Chem. Phys.*, 2015, **17**, 32173–32182.

5 M. Reiher, N. Wiebe, K. M. Svore, D. Wecker and M. Troyer, *Proc. Natl. Acad. Sci. U. S. A.*, 2017, **114**, 7555–7560.

6 S. J. Weininger, *Annals of Science*, 2015, **72**, 242–257.

7 J. A. N. F. Gomes and R. B. Mallion, *Chem. Rev.*, 2001, **101**, 1349–1383.

8 A. Kekulé, *Bulletin mensuel de la Société Chimique de Paris*, 1865, **3**, 98–110.

9 M. Solà, *Frontiers in Chemistry*, 2017, **5**, 22.

10 E. Hückel, *Zeitschrift für Physik*, 1931, **70**, 204–286.

11 R. Breslow, *Accounts of Chemical Research*, 1973, **6**, 393–398.

12 T. Bally and S. Masamune, *Tetrahedron*, 1980, **36**, 343–370.

13 E. G. Lewars, *Chemical Reviews*, 1983, **83**, 519–534.

14 G. Maier, *Angewandte Chemie International Edition in English*, 1988, **27**, 309–332.

15 D. J. Cram, M. E. Tanner and R. Thomas, *Angewandte Chemie International Edition in English*, 1991, **30**, 1024–1027.

16 D. R. Hartree, *Mathematical Proceedings of the Cambridge Philosophical Society*, 1928, **24**, 111–132.

17 D. R. Hartree and W. Hartree, *Proceedings of the Royal Society of London. Series A - Mathematical and Physical Sciences*, 1935, **150**, 9–33.

18 W. Pauli, *Zeitschrift für Physik*, 1925, **31**, 765–783.

19 P. Lykos and G. W. Pratt, *Reviews of Modern Physics*, 1963, **35**, 496–501.

20 C. C. Roothaan, *Reviews of Modern Physics*, 1960, **32**, 179–185.

21 D. M. Hanson, E. Harvey, R. Sweeny, T. J. Zielinski, J. Simons and G. Ackland, *Hartree-Fock Equations are Solved by the Self-Consistent Field Method - Chemistry LibreTexts*, 2019, `https://chem.libretexts.org/Courses/University_of_California_Davis/UCD_Chem_110A%3A_Physical_Chemistry__I/UCD_Chem_110A%3A_Physical_Chemistry_I_(Koski)/Text/08%3A_Multielectron_Atoms/8.03%3A_Hartree-Fock_Equations_are_Solved_by_the_Self-Consistent_Field_Method`.

22 S. M. Blinder, *American Journal of Physics*, 1965, **33**, 431–443.

23 R. Van Noorden, B. Maher and R. Nuzzo, *Nature News Feature*, 2014, 550–553.

24 R. Haunschild, A. Barth and B. French, *Journal of Cheminformatics*, 2019, **11**, 72.

25 J. M. Seminario, *An introduction to density functional theory in chemistry*, Elsevier, 1995, vol. 2, pp. 1–27.

26 J. P. Perdew, K. Burke and M. Ernzerhof, *Physical Review Letters*, 1996, **77**, 3865–3868.

27 C. Adamo and V. Barone, *Journal of Chemical Physics*, 1999, **110**, 6158–6170.

28 C. Adamo and V. Barone, *Journal of Chemical Physics*, 1999, **108**, 664–675.

29 *DFT*, 2006, `https://www.cup.uni-muenchen.de/ch/compchem/energy/dft1.html`.

30 M. D. Hanwell, D. E. Curtis, D. C. Lonie, T. Vandermeerschd, E. Zurek and G. R. Hutchison, *J. Cheminform.*, 2012, **4**, 17.

31 *Jmol: an open-source Java viewer for chemical structures in 3D*, `http://www.jmol.org/`.

32 J. Wang, R. M. Wolf, J. W. Caldwell, P. A. Kollman and D. A. Case, *J. Comput. Chem.*, 2004, **25**, 1157–1174.

33 T. A. Halgren, *J. Comput. Chem.*, 1996, **17**, 490–519.

34 N. M. O'Boyle, M. Banck, C. A. James, C. Morley, T. Vandermeersch and G. R. Hutchison, *Journal of Cheminformatics*, 2011, **3**, 33.

35 *The Open Babel Package, version 2.3.1*, `http://openbabel.org`.

36 G. Schaftenaar, E. Vlieg and G. Vriend, *J. Comput. Aided. Mol. Des.*, 2017, **31**, 789–800.

37 H. B. Schlegel, *Mod. Electron. Struct. Theory Part 1*, 1995, ch. 8, pp. 459–500.

38 M. Born and R. Oppenheimer, *Annalen der Physik*, 1927, **389**, 457–484.

39 P. V. R. Schleyer, C. Maerker, A. Dransfeld, H. Jiao and N. J. Van Eikema Hommes, *J. Am. Chem. Soc.*, 1996, **118**, 6317–6318.

40 R. Herges and D. Geuenich, *J. Phys. Chem. A*, 2001, **105**, 3214–3220.

41 D. Geuenich, K. Hess, F. Köhler and R. Herges, *Chem. Rev.*, 2005, **105**, 3758–3772.

42 L. Pauling, *J. Chem. Phys.*, 1936, **4**, 673–677.

43 K. Y. Lonsdale, *Proc. R. Soc. London. Ser. A - Math. Phys. Sci.*, 1937, **159**, 149–161.

44 W. Bragg, *Proc. R. Soc. London. Ser. A - Math. Phys. Sci.*, 1937, **159**, 149–161.

45 G. Monaco and R. Zanasi, *Phys. Chem. Chem. Phys.*, 2016, **18**, 11800–11812.

46 F. Sondheimer, *Accounts of Chemical Research*, 1972, **5**, 81–91.

47 R. Zanasi, P. Lazzeretti, M. Malagoli and F. Piccinini, *The Journal of Chemical Physics*, 1995, **102**, 7150–7157.

48 H. Fliegl, S. Taubert, O. Lehtonen and D. Sundholm, *Physical Chemistry Chemical Physics*, 2011, **13**, 20500–20518.

49 D. Sundholm, H. Fliegl and R. J. Berger, *Wiley Interdisciplinary Reviews: Computational Molecular Science*, 2016, **6**, 639–678.

50 G. Merino, T. Heine and G. Seifert, *Chem. - A Eur. J.*, 2004, **10**, 4367–4371.

51 P. v. R. Schleyer, H. Jiao, N. J. R. v. E. Hommes, V. G. Malkin and O. L. Malkina, *J. Am. Chem. Soc.*, 1997, **119**, 12669–12670.

52 P. Von Ragué Schleyer, B. Kiran, D. V. Simion and T. S. Sorensen, *J. Am. Chem. Soc.*, 2000, **122**, 510–513.

53 P. Von Ragué Schleyer, M. Manoharan, Z. X. Wang, B. Kiran, H. Jiao, R. Puchta and N. J. Van Eikema Hommes, *Org. Lett.*, 2001, **3**, 2465–2468.

54 H. Fallah-Bagher-Shaidaei, C. S. Wannere, C. Corminboeuf, R. Puchta and P. V. Schleyer, *Organic Letters*, 2006, **8**, 863–866.

55 A. C. Tsipis, I. G. Depastas and C. A. Tsipis, *Symmetry*, 2010, **2**, 284–319.

56 R. Báez-Grez, L. Ruiz, R. Pino-Rios and W. Tiznado, *RSC Advances*, 2018, **8**, 13446–13453.

57 C. Corminboeuf, T. Heine and J. Weber, *Phys. Chem. Chem. Phys.*, 2003, **5**, 246–251.

58 Z. Chen, C. S. Wannere, C. Corminboeuf, R. Puchta, P. Von and R. Schleyer, *Chemical Reviews*, 2005, **105**, 3842–3888.

59 A. Stanger, *J. Org. Chem.*, 2006, **71**, 883–893.

60 E. Clar, *The Aromatic Sextet*, J. Wiley, 1972.

61 *Erich Clar Page Glasgow University Chemistry Department*, `http://www.chem.gla.ac.uk/staff/alanc/clar.htm`.

62 C. H. Suresh and S. R. Gadre, *Journal of Organic Chemistry*, 1999, **64**, 2505–2512.

63 B. J. Lampkin, P. B. Karadakov and B. VanVeller, *Angewandte Chemie International Edition*, 2020, **59**, 19275–19281.

64 E. Clar, *Polycyclic Hydrocarbons*, Springer Berlin Heidelberg, Berlin, 1964, vol. 2.

65 R. F. W. Bader, *Acc. Chem. Res.*, 1985, **18**, 9–15.

66 F. London, *J. Phys. le Radium*, 1937, **8**, 397–409.

67 W. E. Lorensen and H. E. Cline, *SIGGRAPH Comput. Graph.*, 1987, **21**, 163–169.

68 M. J. Frisch, G. W. Trucks, H. B. Schlegel, G. E. Scuseria, M. A. Robb, J. R. Cheeseman, G. Scalmani, V. Barone, G. A. Petersson, H. Nakatsuji, X. Li, M. Caricato, A. V. Marenich, J. Bloino, B. G. Janesko, R. Gomperts, B. Mennucci, H. P. Hratchian, J. V. Ortiz, A. F. Izmaylov, J. L. Sonnenberg, D. Williams-Young, F. Ding, F. Lipparini, F. Egidi, J. Goings, B. Peng, A. Petrone, T. Henderson, D. Ranasinghe, V. G. Zakrzewski, J. Gao, N. Rega, G. Zheng, W. Liang, M. Hada, M. Ehara, K. Toyota, R. Fukuda, J. Hasegawa, M. Ishida, T. Nakajima, Y. Honda, O. Kitao, H. Nakai, T. Vreven, K. Throssell, J. A. Montgomery, Jr., J. E. Peralta, F. Ogliaro, M. J. Bearpark, J. J. Heyd, E. N. Brothers, K. N. Kudin, V. N. Staroverov, T. A. Keith, R. Kobayashi, J. Normand, K. Raghavachari, A. P. Rendell, J. C. Burant, S. S. Iyengar, J. Tomasi, M. Cossi, J. M. Millam, M. Klene, C. Adamo, R. Cammi, J. W. Ochterski, R. L. Martin, K. Morokuma, O. Farkas, J. B. Foresman and D. J. Fox, *Gaussian~16 Revision C.01*, 2016, Gaussian Inc. Wallingford CT.

69 T. A. Keith and R. F. Bader, *Chem. Phys. Lett.*, 1992, **194**, 1–8.

70 T. A. Keith and R. F. W. Bader, *J. Chem. Phys.*, 1993, **99**, 3669.

71 J. R. Cheeseman, G. W. Trucks, T. A. Keith and M. J. Frisch, *J. Chem. Phys.*, 1996, **104**, 5497–5509.

72 M. Armand and J.-M. Tarascon, *Nature*, 2008, **451**, 652–657.

73 J. B. Goodenough and K. S. Park, *Journal of the American Chemical Society*, 2013, **135**, 1167–1176.

74 K. Zaghib, M. Dontigny, A. Guerfi, P. Charest, I. Rodrigues, A. Mauger and C. M. Julien, *Journal of Power Sources*, 2011, **196**, 3949–3954.

75 R. E. Ciez and J. F. Whitacre, *Journal of Power Sources*, 2016, **320**, 310–313.

76 H. Pan, Y. S. Hu and L. Chen, *Energy and Environmental Science*, 2013, **6**, 2338–2360.

77 M. D. Slater, D. Kim, E. Lee and C. S. Johnson, *Advanced Functional Materials*, 2013, **23**, 947–958.

78 L. Li, Y. Zheng, S. Zhang, J. Yang, Z. Shao and Z. Guo, *Energy and Environmental Science*, 2018, **11**, 2310–2340.

79 J. Y. Hwang, S. T. Myung and Y. K. Sun, *Chemical Society Reviews*, 2017, **46**, 3529–3614.

80 T. Perveen, M. Siddiq, N. Shahzad, R. Ihsan, A. Ahmad and M. I. Shahzad, *Renewable and Sustainable Energy Reviews*, 2020, **119**, 109549.

81 S. Eder, D. Yoo, W. Nogala, M. Pletzer, A. Santana Bonilla, A. J. P. White, K. E. Jelfs, M. Heeney, J. W. Choi and F. Glöcklhofer, *Angewandte Chemie International Edition*, 2020, **59**, 12958–12964.

82 P. B. Karadakov, *Organic Letters*, 2020, **22**, 8676–8680.

83 P. Rothemund, *Journal of the American Chemical Society*, 1935, **57**, 2010–2011.

84 P. Rothemund, *Journal of the American Chemical Society*, 1936, **58**, 625–627.

85 M. F. Perutz, M. G. Rossmann, A. F. Cullis, H. Muirhead, G. Will and A. C. T. North, *Nature*, 1960, **185**, 416–422.

86 *Nature*, 1934, **133**, 321.

87 M. Bröring, S. Köhler and C. Kleeberg, *Angewandte Chemie International Edition*, 2008, **47**, 5658–5660.

88 T. Ito, Y. Hayashi, S. Shimizu, J. Y. Shin, N. Kobayashi and H. Shinokubo, *Angewandte Chemie - International Edition*, 2012, **51**, 8542–8545.

89 A. Ghosh, I. H. Wasbotten, W. Davis and J. C. Swarts, *European Journal of Inorganic Chemistry*, 2005, **2005**, 4479–4485.

90 J. Conradie, C. Foroutan-Nejad and A. Ghosh, *Scientific Reports*, 2019, **9**, 4852.

91 T. E. Wood and A. Thompson, *Chemical Reviews*, 2007, **107**, 1831–1861.

92 T. Yonezawa, S. A. Shafie, S. Hiroto and H. Shinokubo, *Angewandte Chemie International Edition*, 2017, **56**, 11822–11825.

93 P. B. Karadakov and K. E. Horner, *Journal of Physical Chemistry A*, 2013, **117**, 518–523.

94 P. B. Karadakov, P. Hearnshaw and K. E. Horner, *Journal of Organic Chemistry*, 2016, **81**, 11346–11352.

95 G. Zhang and M. Mastalerz, *Chemical Society Reviews*, 2014, **43**, 1934–1947.

96 A. Galan and P. Ballester, *Chemical Society Reviews*, 2016, **45**, 1720–1737.

97 M. Yoshizawa and M. Yamashina, *Chemistry Letters*, 2017, **46**, 163–171.

98 M. Yamashina, Y. Tanaka, R. Lavendomme, T. K. Ronson, M. Pittelkow and J. R. Nitschke, *Nature*, 2019, **574**, 511–

515.
99 Y. Ni, T. Y. Gopalakrishna, H. Phan, T. Kim, T. S. Herng, Y. Han, T. Tao, J. Ding, D. Kim and J. Wu, *Nature Chemistry*, 2020, **12**, 242–248.
100 E. Kayahara, T. Iwamoto, H. Takaya, T. Suzuki, M. Fujitsuka, T. Majima, N. Yasuda, N. Matsuyama, S. Seki and S. Yamago, *Nature Communications*, 2013, **4**, 2694.
101 K. Matsui, Y. Segawa and K. Itami, *Journal of the American Chemical Society*, 2014, **136**, 16452–16458.
102 X. S. Ke, T. Kim, Q. He, V. M. Lynch, D. Kim and J. L. Sessler, *Journal of the American Chemical Society*, 2018, **140**, 16455–16459.
103 J. Oh, Y. M. Sung, H. Mori, S. Park, K. Jorner, H. Ottosson, M. Lim, A. Osuka and D. Kim, *Chem*, 2017, **3**, 870–880.
104 T. Soya, H. Mori, Y. Hong, Y. H. Koo, D. Kim and A. Osuka, *Angewandte Chemie International Edition*, 2017, **56**, 3232–3236.
105 W.-Y. Cha, T. Kim, A. Ghosh, Z. Zhang, X.-S. Ke, R. Ali, V. M. Lynch, J. Jung, W. Kim, S. Lee, S. Fukuzumi, J. S. Park, J. L. Sessler, T. K. Chandrashekar and D. Kim, *Nature Chemistry*, 2017, **9**, 1243–1248.